Size effect on the magnetic properties of antiferromagnetic $La_{0.2}Ca_{0.8}MnO_3$ nanoparticles

V. Markovich,[1,*] I. Fita,[2,3] A. Wisniewski,[2] D. Mogilyansky,[4] R. Puzniak,[2] L. Titelman,[4] C. Martin,[5] and G. Gorodetsky[1]

[1]*Department of Physics, Ben-Gurion University of the Negev, 84105 Beer-Sheva, Israel*

[2]*Institute of Physics, Polish Academy of Sciences, Aleja Lotnikow 32/46, 02-668 Warsaw, Poland*

[3]*Donetsk Institute for Physics & Technology, National Academy of Sciences, 83114 Donetsk, Ukraine*

[4]*Institute of Applied Research, Ben-Gurion University of the Negev, 84105 Beer-Sheva, Israel*

[5]*Laboratoire CRISMAT, UMR 6508, ENSICAEN/CNRS, 14050 Caen Cedex 4, France*

(Received 26 August 2009; revised manuscript received 21 January 2010; published 25 March 2010)

Magnetic properties of electron-doped $La_{0.2}Ca_{0.8}MnO_3$ manganite nanoparticles with average particle size ranging from 15 to 37 nm, prepared by the glycine-nitrate method, have been investigated in temperature range 5–300 K and in magnetic fields up to 90 kOe. A monotonous enhancement of weak ferromagnetism linked to the reduction in the particle size was observed for all nanoparticles. Magnetic hysteresis loops also indicate size-dependent exchange bias effect displayed by horizontal and vertical shifts in field-cooled processes. The magnetization data reveal two ferromagnetic components: first one appears at $T \sim 200$ K and may be attributed to surface magnetization and second one appears as a result of spin canting of antiferromagnetic core or is developed at some interfaces inside nanoparticles. Time evolution of magnetization recorded in magnetic fields after the field cooling to low temperatures exhibits a very noisy behavior that may be caused by formation of collective state of nanoparticles with no clear tendency to reach equilibrium state. Magnetic properties of the nanoparticle samples are compared with those of the bulk $La_{0.2}Ca_{0.8}MnO_3$.

DOI: 10.1103/PhysRevB.81.094428 PACS number(s): 75.47.Lx, 75.50.Tt, 75.70.Rf

I. INTRODUCTION

The manganites with a general formula $R_{1-x}A_xMnO_3$, where R and A are rare- and alkaline-earth ions, respectively, have been actively investigated over the past decade because of their colossal magnetoresistance.[1,2] It is well accepted that the double-exchange (DE) ferromagnetic (FM) interaction occurs via hopping of spin-polarized e_g electrons, between Mn^{3+} and Mn^{4+} ions resulting in the formation of FM metallic (FMM) clusters imbedded in antiferromagnetic (AFM) matrix. The presence of magnetic states, for which excess carriers remain localized close to impurity or manganese ion, may energetically favor an interaction of spins similar to superexchange. This may yield FM insulating or AFM phases. Coexisting FMM domains and AFM insulating regions were found in diverse manganites nanoparticles, characterized by their unique core/shell spin configuration and magnetic interactions. While the core may exhibit various magnetic phases and charge ordering (CO), occurring in the bulk, the shell being magnetically and structurally incommensurate with the bulk exhibits in general other FM, AFM, or paramagnetic (PM) spin structures. Incommensurate magnetization of the core and the shell and magnetic interactions between the particles may set off new magnetic and electronic states in addition to those in the bulk. Surface magnetism inevitably existing in nanoparticles may therefore drastically affect magnetic properties.

Recent studies of electron doped $La_{1-x}Ca_xMnO_3$ ($x > 0.5$) (Refs. 3–5) nanoparticles have demonstrated relaxation effects of superexchange interaction in the surface layer and formation of FM-like shell, whose thickness increases with decreasing particle size. Similar FM tendency for nanosized charge-ordered $Nd_{0.5}Ca_{0.5}MnO_3$, $Pr_{0.65}Ca_{0.35}MnO_3$, and $Pr_{0.5}Ca_{0.5}MnO_3$ manganites (Refs. 6–8, respectively) was also found at the surface of particles. Phenomenological model and Monte Carlo studies[9] have shown an enhancement of surface-charge density and confirmed a suppression of AFM/CO phase and an emergence of FM order near the surface. It was reported that for $La_{0.4}Ca_{0.6}MnO_3$ reducing in the particle size to 20–60 nm results in full suppression of AFM/CO order and formation of FM-like ordering with high enough spontaneous magnetization of ~ 1 μ_B/f.u. corresponding to $\sim 30\%$ of FM fraction.[5] Rozenberg *et al.*[10] criticized this finding and suggested that AFM/CO state is somewhat reduced in ~ 17 nm particles in contradiction to the results of Lu *et al.*[5] This may be explained by extrinsic nonstoichiometry effects.

Externally induced strain or internal strain in nanoparticles may account for their magnetic behavior. Strong magnetic interactions, e.g., particle-particle exchange interactions may also play a role in their magnetic properties. This kind of coupling occurs usually at FM/AFM interface, manifesting itself by an exchange bias (EB) effect that shifts the magnetization hysteresis loop. In recent years, the effect of exchange bias attracted a considerable interest in spintronics.[11–14] Most experimental and theoretical studies of EB have been performed almost exclusively for FM/AFM multilayers and FM nanoparticles embedded in an AFM matrix.[11] In addition to FM/AFM systems, the EB effect was also observed for samples containing a ferrimagnet (FI) or a spin-glass (SG) phase (FI/AFM, FM/FI, FI/SG, and AFM/SG).[11] Recently, the EB effect was observed in phase separated $Pr_{1/3}Ca_{2/3}MnO_3$ and $Y_{0.2}Ca_{0.8}MnO_3$ manganites (Refs. 12 and 13) and $La_{1-x}Sr_xCoO_3$ cobaltites (Ref. 14) due to intrinsic interface exchange coupling between the FM nanodroplets and surrounding AFM matrix[12,13] or SG regions.[14] In the case of nanosized AFM manganites, the variation of the superexchange interaction at the surface layer allows a formation of FM shells, resulting in a natural AFM/FM interfaces and EB effect.[9,15–17]

Detailed neutron powder diffraction, electron spin resonance, and magnetization studies of the phase diagram of $La_{1-x}Ca_xMnO_3$ in electron-doped range have shown the existence of four phase boundaries $x=0.5$, $x=2/3$, $x=0.8-0.85$, and $x=1$ at which the compound forms a distinct crystallographic and magnetic phases.[18–20] The compound with doping level $x=0.8$ is of special interest since it displays orbital ordering (OO) but no charge ordering. It should be noted that neutron-diffraction studies of $La_{0.2}Ca_{0.8}MnO_3$ show that the temperatures of AFM ordering (T_N) and of structural transition (a monoclinic distortion) at orbital ordering (T_{OO}) coincide.[18]

In this paper, we present magnetic studies of $La_{0.2}Ca_{0.8}MnO_3$ (LCMO) nanoparticles with average particle size ranging from 15 to 37 nm, in the temperature range 5–300 K and in magnetic field up to 90 kOe. With decreasing particle size the OO transition shifts toward low temperatures while the spontaneous magnetization increases and approaches a value of 0.026 μ_B/f.u. at $T=5$ K for the smallest 15 nm particles. Upon field cooling, the particles display size-dependent exchange bias effect. It was found that coercivity and exchange bias effect progressively diminish with increasing temperature and fully disappear at ~100 K, while surface ferromagnetism remains up to $T\sim 200$ K.

II. EXPERIMENTAL

Nanocrystalline LCMO particles have been prepared by the glycine-nitrate method, previously used for preparation of the nanosized $La_{0.7}Ca_{0.3}MnO_3$ powder.[21] A stoichiometric amount of $La(NO_3)_3\cdot 6\ H_2O$, $Ca(NO_3)_2\cdot 6\ H_2O$, $Mn(NO_3)_2\cdot 4\ H_2O$, and glycine ($C_2H_5NO_2$) were dissolved in water to form the precursor solution. A molar ratio of ~0.5 between glycine and nitrate was found appropriate for producing a single-phase perovskite compound. The precursor solution of each nitrate with glycine was mixed well by stirring during 4 h, and then all solutions were merged together, and resulting solution was mixed by stirring during 15 h, resulting in homogeneous mixture. This solution was heated using a hot plate up to ~100 °C for a 1.5–2 h to dehydrate. Afterwards, the solution became a transparent viscous gel. Subsequent heating of this gel to $T\sim 300$ °C results in the autoignition with short combustion of few seconds with formation of a black porous ash of $La_{0.2}Ca_{0.8}MnO_3$ compound. Then the powder in low layer was heated with rate 5 °C/min to desired temperatures (750–1100 °C) in the flow of 40% O_2 and 60% Ar for 1 h to get a series of LCMO nanocrystalline powders having varying grain sizes.

The x-ray diffraction (XRD) data were collected on Philips 1050/70 powder diffractometer with a graphite monochromator on diffracted beam providing $K\alpha$ radiation ($\lambda=1.541$ Å) and operating at $V=40$ kV and $I=30$ mA. The x-ray diffraction patterns were then treated by using the FULLPROF computer program in order to fit structure parameters and crystallites size. The nanoparticles were also characterized by transmission electron microscopy (TEM) equipped with energy-dispersive x-ray spectroscopy (EDS) facilities. Cylinder-shape samples having a diameter of 2.4 mm and height of 3.0 mm prepared by compaction of

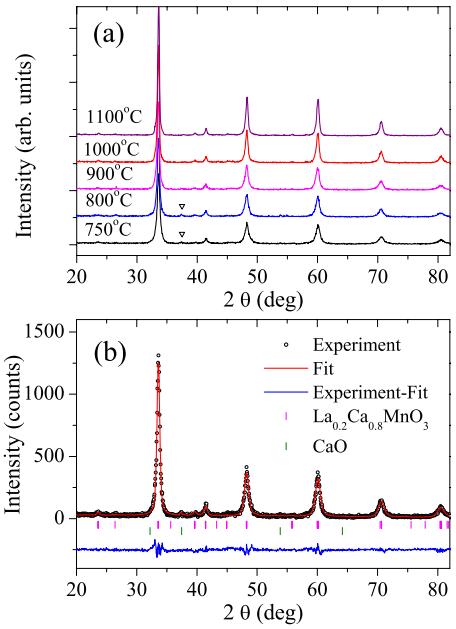

FIG. 1. (Color online) (a) XRD spectra of samples LCMO15, LMO20, LCMO23, LCMO32, and LCMO37 samples, annealed at 750, 800, 900, 1000, and 1100 °C, respectively, (the peak belonging to CaO is signed by triangle); (b) Rietveld plot for LCMO15 sample. The data points are indicated by open circles, the calculated and difference patterns are shown by solid lines. The Bragg positions of the reflections of manganite and CaO are indicated by vertical lines below the pattern.

$La_{0.2}Ca_{0.8}MnO_3$ nanoparticle powder under pressure of ~5 kbar at room temperature were used in our magnetic measurements. The measurements, using PAR (Model 4500) vibrating sample magnetometer (VSM), were completed in the temperature range 5–290 K and magnetic fields up to 15 kOe, applied perpendicularly to the rotation axis of the samples. The measurements of ac susceptibility in the temperature range 5–300 K as well as the measurements of magnetization in high magnetic field up to 90 kOe were performed using the magnetic option of the physical property measurement system (PPMS) of Quantum Design.

III. RESULTS AND DISCUSSION

The XRD pattern of the as-prepared sample presents a mixture of perovskite and amorphous phases. After annealing at $T>700$ °C an almost pure orthorhombic perovskite phase was obtained and only few percent (~3 wt. %) of calcium oxide (CaO) remained in the samples annealed at $T=750$ and 800 °C. It is well known that CaO is diamagnetic insulating compound with diamagnetic susceptibility equal to -0.27×10^{-6} emu/g.[22] The XRD patterns of the samples calcined at various temperatures (750, 800, 900, 1000, and 1100 °C) are shown in Fig. 1(a). The fit for samples annealed at 750 °C is shown in Fig. 1(b). The average crystallite sizes $\langle D\rangle$ and the lattice parameters (listed in Table I) were calculated using Debye-Scherrer equation. These samples will be denoted herein by: LCMO15, LCMO20, etc. The size of the nanoparticles was also con-

TABLE I. Crystalline size and lattice parameters of the $La_{0.2}Ca_{0.8}MnO_3$ samples annealed at various temperatures.

Temperature of calcination (°C)	Crystalline size (nm)	Lattice parameters (Å)		
		a	*b*	*c*
750	15 ± 1	5.344(2)	7.533(3)	5.341(2)
800	20 ± 1	5.343(2)	7.531(2)	5.342(2)
900	23 ± 1	5.340(1)	7.531(2)	5.335(1)
1000	32 ± 2	5.342(1)	7.532(1)	5.338(1)
1100	37 ± 2	5.341(1)	7.532(1)	5.338(1)

firmed by TEM and high-resolution TEM. Figure 2 shows the (a) bright-field and (b) high-resolution images for LCMO15 sample. It was found that the size of LCMO15 single-isolated nanoparticle is equal to 15 ± 1 nm. The EDS analysis confirmed the composition and homogeneous distribution of the constituent elements: nominal atomic values La:Ca:Mn=0.2:0.8:1.0. The approximate value of oxygen content determined by EDS analysis is equal to 2.99 ± 0.04. It should be noted that the lattice parameters for all samples are similar to the ones of $La_{0.2}Ca_{0.8}MnO_3$ ceramics.[23]

Field-cooled (FC) magnetization (M_{FC}) and zero-field-cooled (ZFC) (M_{ZFC}) magnetization curves for LCMO37 and LCMO15 samples, recorded at an applied field $H=10$ kOe, are shown in Figs. 3(a) and 4(a). It should be noted that for bulk $La_{0.2}Ca_{0.8}MnO_3$, the temperature of magnetization maximum is 214 K, corresponding to T_{OO}.[18,20] It appears that with decreasing particle size T_{OO} shifts toward lower temperatures. Moreover, the temperature dependence of the magnetization [Figs. 3(a) and 4(a)] and its derivative [Figs. 3(b) and 4(b)] presents some other noticeable features. As the temperature decreases below ~100 K, the magnetization displays considerable increase while ZFC and FC curves split off significantly, indicating the onset of weak FM moment at T_C(on). The inverse magnetization for both samples exhibits a linear temperature dependence above T_{OO} implying a Curie-Weiss behavior $\chi=C/(T-\theta)$, where C is the Curie constant and θ is the paramagnetic Curie temperature. Since the temperature range where χ obeys Curie-Weiss law is quite narrow (240–300 K), linear fitting in this range gives only a rough estimation of θ. Therefore, as one may expect,

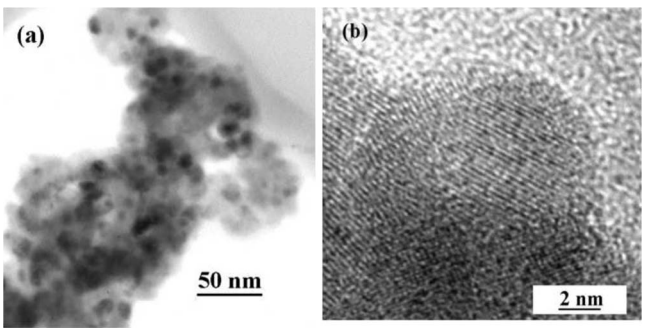

FIG. 2. (a) TEM bright-field and (b) high-resolution images of the sample LCMO15.

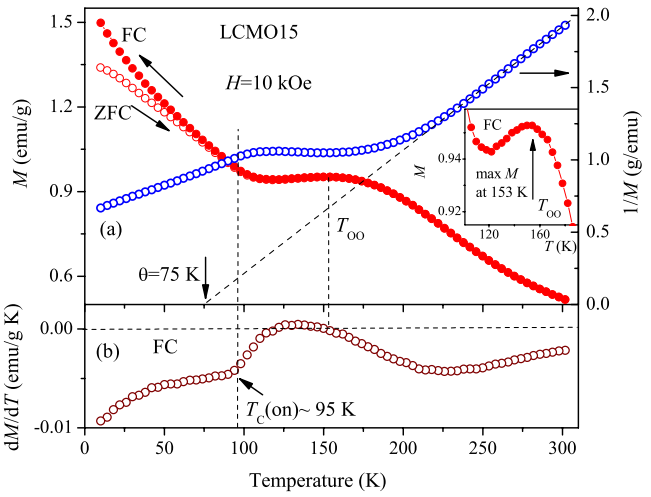

FIG. 3. (Color online) (a) Temperature dependence of zero-field-cooled M_{ZFC} (open symbols) and field-cooled M_{FC} (solid symbols) magnetization of LCMO15 sample in magnetic field $H=10$ kOe. $1/M$ vs temperature curve. Dash line presents result of linear fitting. Inset shows FC magnetization of LCMO15 sample in the vicinity of T_{OO} in an extended scale; (b) dM_{FC}/dT vs temperature for LCMO15 sample.

the values $\theta=75$ K for LCMO15 and $\theta=78$ K for LCMO37 [see Figs. 3(a) and 4(a)] do not differ significantly from the value of $\theta=66$ K observed for bulk $La_{0.2}Ca_{0.8}MnO_3$. The later was derived from electron magnetic resonance measurements carried out in the temperature range 240–500 K.[24]

In order to get a better understanding of the magnetic behavior near T_{OO}, T_N, and T_C(on), we have measured the temperature dependence of ac susceptibility of bulk $La_{0.2}Ca_{0.8}MnO_3$ sample (Fig. 5) and LCMO15, LCMO23, and LCMO37 samples (Fig. 6) as well. Some of the results obtained for the bulk sample of $La_{0.2}Ca_{0.8}MnO_3$ are de-

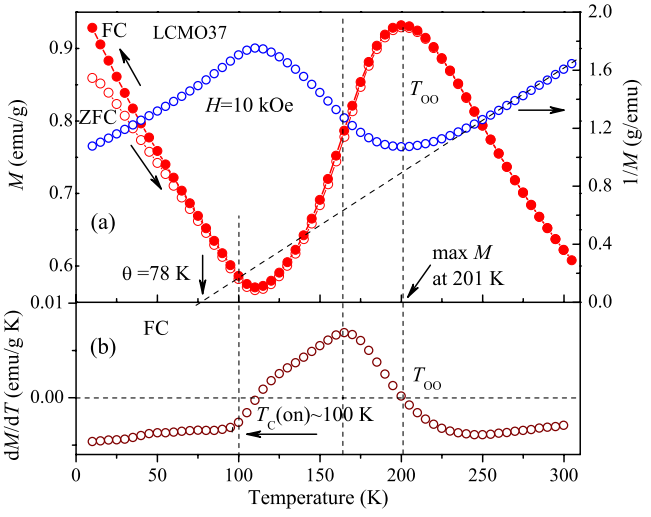

FIG. 4. (Color online) (a) Temperature dependence of zero-field-cooled M_{ZFC} (open symbols) and field-cooled M_{FC} (solid symbols) magnetization of LCMO37 sample in magnetic field $H=10$ kOe. $1/M$ vs temperature curve. Dash line presents result of linear fitting. (b) dM_{FC}/dT vs temperature for LCMO37 sample.

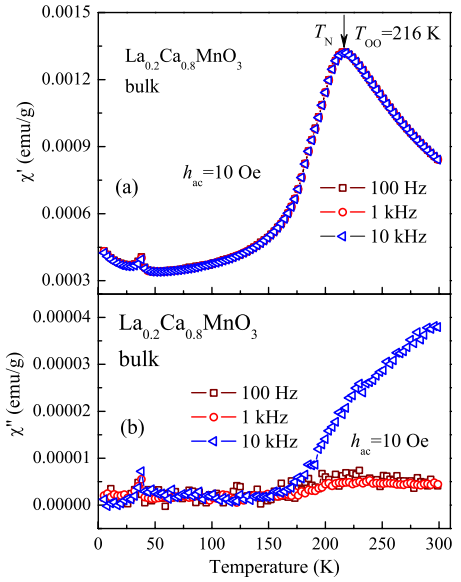

FIG. 5. (Color online) Temperature dependence of a (a) real (χ') and (b) imaginary (χ'') components of ac susceptibility for $La_{0.2}Ca_{0.8}MnO_3$ polycrystalline sample, measured during heating, at different frequencies of 100, 1000, and 10 000 Hz and in magnetic ac field of 10 Oe.

scribed in Ref. 20. One may directly realize several worth noting features. First, the resemblance between the real part of the ac susceptibility χ' and magnetization $M(T)$ of the bulk $La_{0.2}Ca_{0.8}MnO_3$ sample (see Fig. 4 in Ref. 20). In both cases the peaks in $\chi'(T)$ and $M(T)$ occur practically at the same temperature T_{OO}/T_N. While χ' for the bulk $La_{0.2}Ca_{0.8}MnO_3$ was found to be frequency independent at all temperatures, see Fig. 5, the ac susceptibility of the nanoparticles (Fig. 6) shows a well-pronounced frequency dependence and a double-peak curve. Both peaks shift toward lower temperatures with decreasing particle size, see Fig. 6. The higher temperature susceptibility peaks (Fig. 6) and the maximum in dM/dT [Figs. 3(b) and 4(b)] occur at the same temperatures, therefore one may tentatively attribute this behavior to AFM ordering. It is well known that, the susceptibility of paramagnets increases monotonously with decreasing temperature. On the other hand, antiferromagnets show a decrease of susceptibility with a decrease of temperature, below the transition temperature from PM to AFM state. Consequently, a distinct signature is expected at PM-AFM transition.[25] Therefore, we associate high-temperature peak in the temperature dependence of ac susceptibility with the Néel temperature T_N, see Figs. 5 and 6. It is clearly seen from Figs. 5 and 6 that the T_N of bulk sample is much larger than that of nanoparticles and the Néel temperature of the nanoparticles decreases monotonously with decreasing particle size from $T_N \approx 173$ K for LCMO37 to $T_N \approx 143$ K for LCMO15. It should be also noted that χ' and χ'' exhibit a weak frequency dependence for the relatively large particles [see Figs. 6(a) and 6(d)], but well-pronounced dependence for smaller particles, see Figs. 6(b)–6(e) and 6(c)–6(f). Below T_C(on) [Figs. 3(a) and 4(a)] all nanoparticle samples show not only bifurcation between the ZFC and FC magnetization but also frequency-dependent peak in χ' (see Fig. 6).

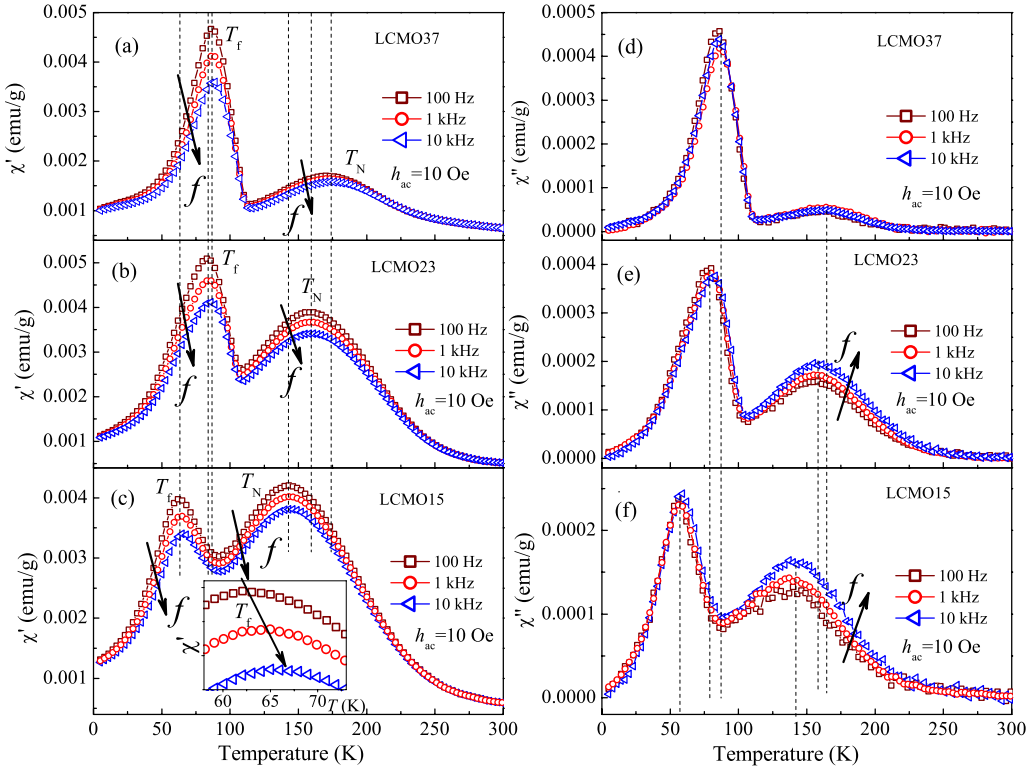

FIG. 6. (Color online) (a)–(c) Temperature dependence of a real component of ac susceptibility χ' of LCMO37, LCMO23, and LCMO15 samples measured during heating at different frequencies of 100, 1000, and 10 000 Hz and in magnetic ac field of 10 Oe; (d)–(f) $\chi''(T)$ curves for LCMO37, LCMO23, and LCMO15 samples, registered during heating, at 100, 1000, and 10 000 Hz in magnetic field of 10 Oe.

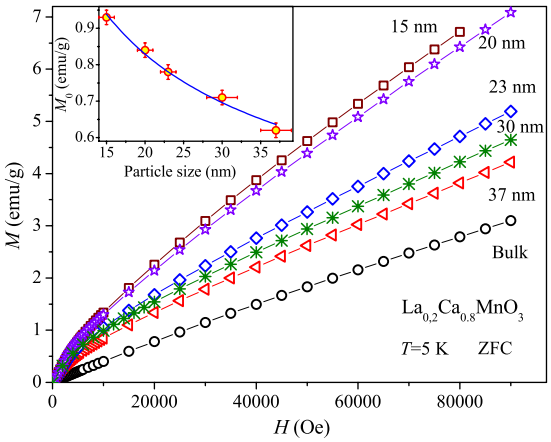

FIG. 7. (Color online) Magnetic field dependences of magnetization measured at $T=5$ K for LCMO bulk and nanoparticle samples. Inset shows the variation of spontaneous moment with particle size. Solid line is the result of fitting of the expression $M_0=A/D^{\alpha}$ to the experimental points. The parameters of the fitting are: $A=3.01\pm0.25$ and $\alpha=0.43\pm0.02$.

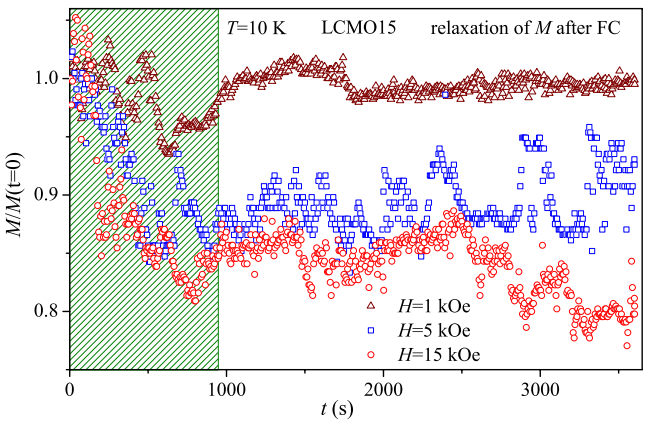

FIG. 8. (Color online) Relaxation of magnetization after cooling to 10 K in magnetic field of 1, 5, and 15 kOe for LCMO15 sample. The values of magnetization are normalized to the value of magnetization at $t=0$.

The temperature at which the peak occurs shifts to lower temperature with decreasing particle size [see Figs. 6(a)–6(c)] and shifts to higher temperatures with increasing frequency [see inset in Fig. 6(c)]. The frequency dependence of the ac susceptibility at the lower temperature is a direct indication of slow spin dynamics leading us to associate this peak with the freezing temperature of FM clusters, T_f. Indeed, such a frequency-dependent temperature shift is a reminiscence of a spin/cluster glass-like behavior and it can be characterized by the factor $K=\Delta T_f/T_f\Delta(\log\omega)$, where T_f refers to the temperature of the maximum of χ' and ΔT_f is the temperature shift at a given frequency. The calculated K factor for LCMO15, LCMO23, and LCMO37 samples varies in the range 0.012–0.026, falling in the range of the values typical for spin glasses.[26]

The evolution of magnetic properties with decreasing particle size is also evidenced by the magnetization M vs H curves recorded at 5 K after ZFC, see Fig. 7. It should be noted that the magnetization curves indicate upon the existence of FM constituents imbedded in the nanoparticles whose relative volume increases with decreasing particle size, namely, an enhancement of FM regions at the expense of AFM phase. The spontaneous magnetization M_0 was evaluated by linear extrapolation of the high field magnetization (≥ 30 kOe) to zero field, e.g., it was found that M_0 for LCMO15 at 5 K is about 0.93 emu/g (0.026 μ_B/f.u.). Spontaneous magnetization increases monotonously with decreasing particle size, see inset of Fig. 7. Since the theoretical value of the magnetization for the fully ordered spins M_{theor} is 3.2 μ_B/f.u., we may conclude that the volume of the FM phase in LCMO15 is only of about 0.8% at 5 K. Moreover, magnetization value of $M=6.71$ emu/g (0.195 μ_B/f.u.) observed for smaller LCMO15 particles at $H=80$ kOe is also much smaller than the M_{theor}. In comparison with recent result for $La_{0.25}Ca_{0.75}MnO_3$ nanoparticles,[16] such a behavior manifests the dominant role of the AFM phase. Recently, a core-shell formation was proposed[9] to describe the magnetic constitution of AFM manganite particles. On this ground, we suggest that the core of all LCMO nanoparticles is AFM below T_N, while the shell may embody a spin-glass-like FM surface layers.[11,27,28]

An unstable magnetization behavior was observed by VSM magnetization measurements of LCMO nanoparticle samples when carried out in magnetic fields of few kilo oersted and temperature range 10–100 K. The variations in the magnetization have attained ~20% of it's initial value (see Fig. 8). In order to get a better understanding of this instability we have recorded time evolution of FC magnetization curves at time intervals of 6 s and elapsed time of 1 h, see Fig. 8. Our data clearly show that the magnetization displays a field-dependent instability and even after 1 h at 10 K the magnetization remains highly noisy. It should be noted that we did not find significant difference in time variation of magnetization observed after quick cooling (~60 K/min) and relatively slow cooling (~3 K/min). There are plenty of examples in the literature[1,29–32] demonstrating relaxation dynamics and time-dependent phenomena in phase-separated manganites, which shares some similarity with spin-glass and cluster-glass systems. The slow-relaxation processes are particularly spectacular: in a spin glass, any field change causes a very long-lasting relaxation of the magnetization. Similarly, time variation of magnetization was observed in phase-separated manganites by the following procedure: the sample was cooled at zero field down to a certain temperature (below the temperature of the irreversibility of ZFC and FC magnetization), and after a waiting time t_w, a small magnetic field was applied (typically between 5 and 50 Oe) and the time-dependent magnetization was recorded.[29–32] Since the magnetization observed during ~1 h in relatively high $H=15$ kOe (after FC in the same magnetic field — no change of the field) (Fig. 8) and $T=10$ K does not exhibit a clear tendency toward some equilibrium value and remains in a highly noise state, we believe that such a behavior characterizes unusual dynamics in electron-doped nanoparticles with very small volume of FM phase. We note that observed dynamics of magnetization (Fig. 8) is not an artifact of our electronics, since the level of the noise of magnetization exceeds the sensitivity of our experimental setup by about two

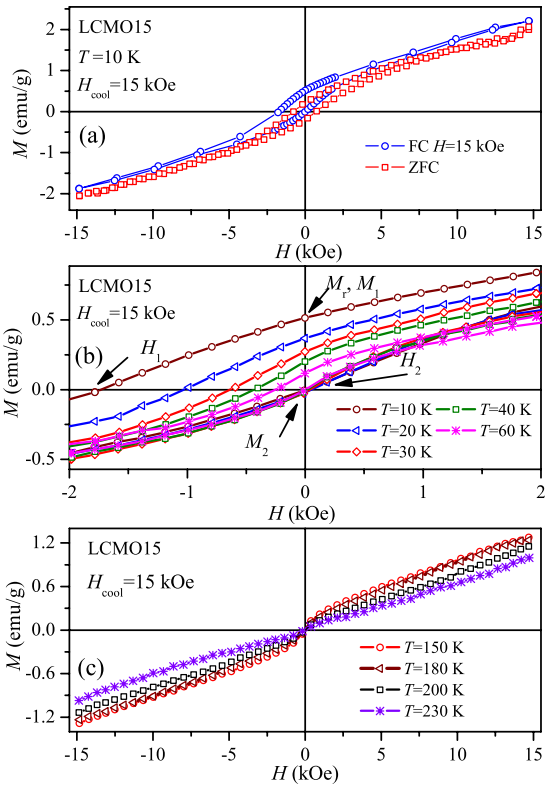

FIG. 9. (Color online) (a) Field dependence of magnetization of LCMO15 at 10 K after ZFC and FC in $H=15$ kOe. [(b) and (c)] Field dependence of magnetization of LCMO15 sample at various temperatures after FC.

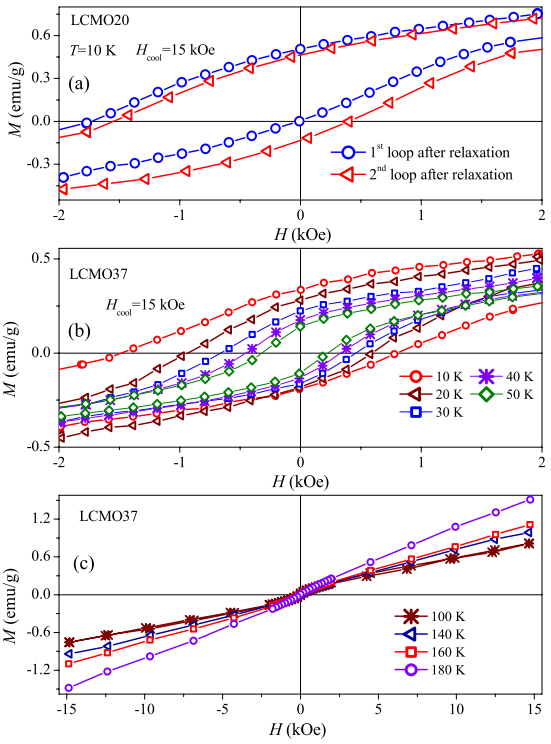

FIG. 10. (Color online) (a) First and second subsequent hysteresis loops recorded after 1 h relaxation followed FC to 10 K for LCMO20 sample. [(b) and (c)] Field dependence of magnetization of LCMO37 sample at various temperatures after FC.

orders of magnitude and change from the LCMO nanoparticle samples to other sample with comparable magnetization in the same chamber under same conditions resulted in complete vanishing of above time-dependent behavior.

It was worth noting that the noisy magnetization observed when measured with VSM but absent when measured with PPMS. The results obtained by PPMS are presented in Figs. 3–7 and those using VSM are shown in Figs. 8–10. VSM and PPMS techniques are methodically different from each other. Data with VSM were carried out a relatively short-time constant, thereby displaying fluctuated magnetization at this frequency. On the other hand, magnetization values with the PPMS are represented by the averaged data points of 25 measurements.

Magnetic hysteresis loops were measured at different temperatures after cooling in zero field (ZFC) and after cooling in an applied field (FC) of $H_{\mathrm{cool}}=15$ kOe. Figure 9(a) presents hysteresis loops recorded for LCMO15 sample at 10 K after ZFC and FC at $H_{\mathrm{cool}}=15$ kOe. The shifts along both magnetic field and magnetization axes are clearly seen for FC but absent in ZFC process. The above difference between ZFC and FC magnetic hysteresis loops manifests the phenomenon of exchange bias. As generally accepted,[11–13] the magnetic field induced shift of the hysteresis loop is defined as $H_{\mathrm{EB}}=-(H_1+H_2)/2$, where H_1 and H_2 are the negative field and the positive field at which the magnetization equals zero. The vertical magnetization shift is defined as $M_{\mathrm{EB}}=(M_1+M_2)/2$, where M_1 and M_2 are the magnetization at the positive and negative points of intersection with $H=0$. Figure 9(b) shows magnetic hysteresis loops recorded at various temperatures after FC to the desired temperature. One can see clearly a decrease of EB effect with increasing temperature with compliance with others observation of the EB effect.[11,12,14,15] At temperatures above 120 K the EB effect practically disappears for LCMO15 sample, likely as the temperature approaches the Néel temperature. It should be emphasized that a spontaneous magnetization tentatively attributed to a presence of the FM phase is still observed up to 210 K. Only above this temperature $M(H)$ curves do not display spontaneous magnetization, see Fig. 9(c). An additional worth noting property of exchange-biased systems is the existence of a so-called training effect, described by the decrease of H_{EB} and M_{EB} when the system is consecutively field cycled at a particular temperature after FC.[11,12,14] The training effect is clearly seen in LCMO nanoparticles, see Fig. 10(a). This figure displays two consecutive M-H loops for LCMO20 sample measured in fields between 15 and −15 kOe at 10 K following 1 h of relaxation. Recent studies[16,17] of the EB effect in manganite nanoparticles have shown a significant particle-size effect regarding H_{EB} and M_{EB}. In particular, Huang *et al.*[16] studied the particle-size dependence of H_{EB} and M_{EB} for $La_{0.25}Ca_{0.75}MnO_3$ particles ranging between 40 and 1000 nm. These authors found a nonmonotonous dependence of H_{EB} and M_{EB} and coercive field H_{C} on particle size, with pronounced maxima for particles with diameter around 80 nm. For our investigated LCMO nanoparticles, we found that both H_{EB} and M_{EB} monotonously decrease with increasing particle size [see Figs.

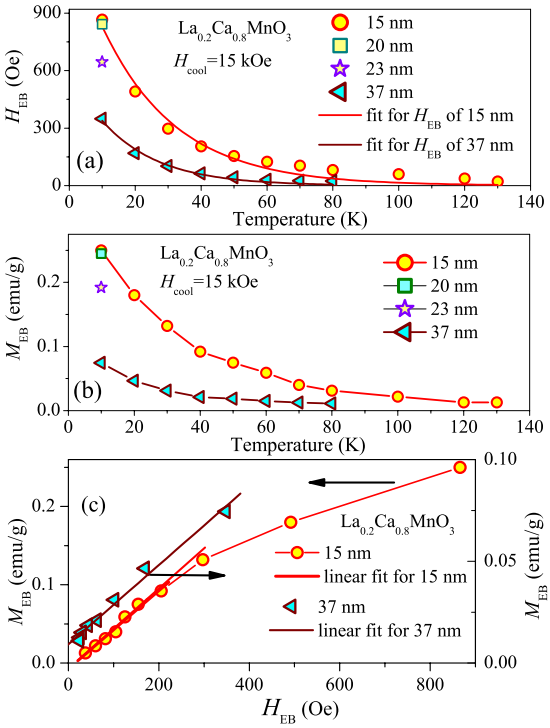

FIG. 11. (Color online) Temperature dependence of (a) H_{EB} and (b) M_{EB} for LCMO15 and LCMO37 samples after FC in 15 kOe. Data for LCMO20 and LCMO23 at 10 K are shown as well. Solid lines in (a) are fits to equation $H_{EB}=H_{EB}(0)\exp(-T/T_0)$. (c) The correlation between M_{EB} and H_{EB}.

11(a) and 11(b)]. The comparison of the magnetization loops recorded for LCMO15 and LCMO37 [Figs. 9(c) and 10(c)] shows some similarities. It is of interest to note that LCMO37 displays small spontaneous moment up to $T\sim 160$ K, even though it vanishes at slightly lower temperatures than that for LCMO15 [Fig. 9(c)].

Figures 11(a) and 11(b) summarize experimental results observed for M_{EB} and H_{EB} for LCMO particles of various size. It is well seen that for 20 nm particles at 10 K the above parameters are practically the same as for smaller LCMO15 particle while further increase in size of nanoparticles results in diminution of both M_{EB} and H_{EB}. Measurements of hysteresis loops for LCMO15 and LCMO37 at FC process (Figs. 9 and 10) show that H_{EB} decays exponentially with temperature. A similar reduction in $H_{EB}(T)$ was observed in multilayers[33] consisting of FM/AFM layers of $La_{1-x}Ca_xMnO_3$ with different Ca doping and also in basically antiferromagnetic $CaMnO_3$ (Ref. 15) and $La_{0.75}Ca_{0.25}MnO_3$ nanoparticles.[16] The temperature variation of $H_{EB}(T)$ for exchange-coupled $La_{1-x}Ca_xMnO_3$ FM/AFM multilayers was described (Ref. 31) by the following expression: $H_{EB}=H_{EB}(0)\exp(-T/T_0)$, where $H_{EB}(0)$ is the extrapolation of H_{EB} to $T=0$ K and T_0 is a constant. Figure 11(a) displays a best fit of the above expression (solid lines) to our experimentally observed H_{EB}. A fairly good agreement is obtained between the above expression and the experimental data observed for LCMO37. For LCMO15, the fit worsen at temperatures $T\geq 60$ K. Recently, Niebieskikwiat and Salamon[12] proposed a simple model to explain intrinsic interface exchange coupling in phase-separated polycrystalline $Pr_{1/3}Ca_{2/3}MnO_3$ manganites, consisting of small FM domains immersed in charge-ordered AFM host. In their approach, H_{EB} was introduced as an asymmetry in the activation energy for the backward and forward switching processes of a single FM domain particles over the anisotropy barrier KV (K is the anisotropy constant and V is the volume of the particles). A simple linear relationship between H_{EB} and M_{EB}: $M_{EB}/M_S \propto H_{EB}$ was obtained, signifying a direct equivalence of both parameters.[12] A linear relationship between M_{EB} and H_{EB} was found for $Pr_{1/3}Ca_{2/3}MnO_3$ polycrystaline compound,[12] $LaMn_{0.7}Fe_{0.3}O_3$ (Ref. 17), $Nd_{1-x}Sr_xCoO_3$ (Ref. 34) polycrystals and for $La_{0.25}Ca_{0.75}MnO_3$ (Ref. 16) and $CaMnO_{3-\delta}$ (Ref. 15) nanoparticles. A linear fit to our experimental data [Fig. 11(c)] shows straightforward correlation between M_{EB} and H_{EB} for LCMO37, while for smaller LCMO15 nanoparticles this relationship is observed only at smaller M_{EB} and H_{EB} (at higher temperatures) and one observes a change from one linear dependence to another one at low temperatures.

It appears from results presented in Figs. 11(a) and 11(b) that the EB effect in LCMO nanoparticles vanishes at $T\sim 100$ K, while spontaneous magnetization exists at much higher temperatures. In order to obtain additional view on the temperature evolution of magnetic phases, we have performed measurements of thermoremanent magnetization (TRM). The TRM of LCMO nanoparticles was measured in the following way: the sample was cooled down to $T=10$ K in magnetic field $H=15$ kOe, then the magnetic field was switched off and after a waiting time of 100 s the magnetization was recorded. It was found that TRM for all nanoparticles behaves in a similar way, namely, it is almost flat at high temperature and below ~ 100 K monotonously increases with decreasing temperature, see Fig. 12(a). The values of the remanent magnetization obtained from hysteresis loops after FC to various temperatures [Figs. 9(b) and 10(b)] agree quite well with the values of thermoremanent magnetization, Figs. 12(b) and 12(c).

As pointed already, the hysteresis loops show the presence of spontaneous magnetization in LCMO nanoparticles, at high $T\sim 200$ K, while the onset of weak FM moment at T_C(on) signifies some additional FM components. Further evidence for the presence of two FM-like components and possibly two exchange couplings may be deduced from the temperature variation of the spontaneous magnetization, observed for LCMO15 and LCMO37, see Figs. 12(b) and 12(c), respectively. As seen in the above figures, a spontaneous magnetization appears at temperatures much higher than T_{OO}, T_N, and T_C(on), and then slowly increases with decreasing temperature up to 100 K, while below this temperature discontinuity in the magnetization changes was observed. Such behavior indicates the presence of two FM contributions, which appear at different temperature regions. The difference between spontaneous magnetization of both LCMO15 and LCMO37 samples [inset in Fig. 12(c)] increases with decreasing temperatures showing a quite abrupt change near T_C(on), which reflects the difference in T_C(on) for both samples.

Let us first discuss the evolution of magnetic phases in bulk and nanosized samples upon cooling from PM state. It

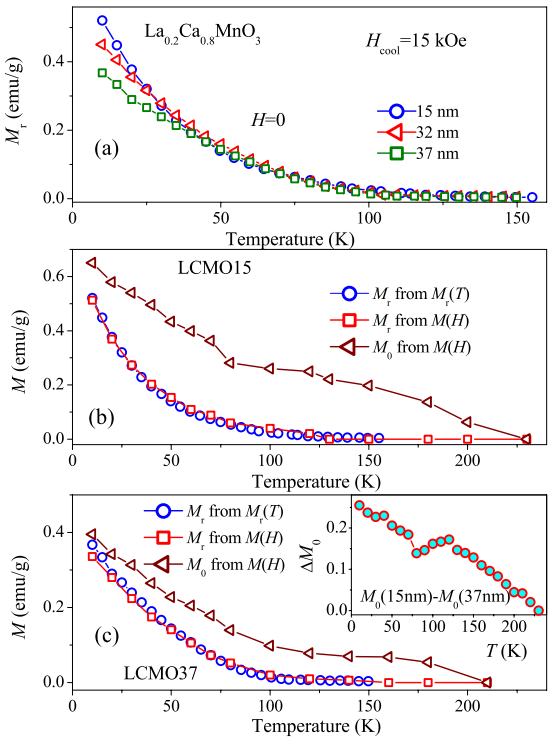

FIG. 12. (Color online) (a) Temperature dependence of TRM for LCMO15, LCMO32, and LCMO37 samples. (b) TRM and remanent magnetization obtained from hysteresis loops at various temperatures for LCMO15 sample. Temperature variation of spontaneous magnetization of LCMO15 sample. (c) TRM and remanent magnetization obtained from hysteresis loops at various temperatures for LCMO37 sample. Temperature variation of spontaneous magnetization of LCMO37 sample. Inset shows the difference between spontaneous magnetization of LCMO15 and LCMO37 samples.

was suggested that the broad magnetization peak in the bulk (at ~210 K) may be attributed to the hopping of the e_g electrons at $T > T_{OO}$, which brings about FM correlations through the DE mechanism. At a decreasing temperature these electrons freeze and the FM fluctuations are replaced by superexchange-driven AFM spin configuration.[18] In the bulk this results in the appearance of a long-range OO below ~210 K, while in the nanoparticles the temperature range of both FM and OO correlations dilates with concomitant shift of T_{OO} toward low T, following a decreasing in particle size. On the other hand, the appearance of spontaneous magnetization at temperatures higher than T_{OO} and a frequency dependence of both components of ac susceptibility around T_{OO} provides indications of an inhomogeneous state. The core-shell model in which FM-like disordered shells and AFM ordered cores form FM cluster glass was suggested[4] for electron-doped LCMO nanocrystals. It is important to note that the surface weak ferromagnetism is a general feature of oxide nanoparticles, including nonmagnetic oxides such as Al_2O_3, ZnO, and CeO_2.[35] The authors of this paper suggest that the room-temperature ferromagnetism observed in the above compounds arises due to exchange interactions between localized electrons' spins related to oxygen vacancies at the surface.[35] Thus, high-temperature FM contribution may be related to surface weak ferromagnetism. Several observations like: "OO peak" even in smaller (15 nm) particles (Fig. 3), weak spontaneous moment at low temperature, a linear dependence of $M(H)$ in high magnetic field up to 90 kOe point out on a stable OO/AFM ground state. Additional indication of stable OO/AFM state is supported by the negligible variation of the paramagnetic Curie temperature θ in comparison with the bulk value. This result completely disagrees with recent observations of full suppression of AFM/CO order and formation of FM-like ordering with high-enough spontaneous magnetization in $La_{0.4}Ca_{0.6}MnO_3$ (Ref. 5) and $Pr_{0.5}Ca_{0.5}MnO_3$ (Ref. 8) nanoparticles. In these particles, the volume of FM fraction for smaller ~20 nm particles approaches a value of 20–30 % of their full volume. It has been recently suggested (Ref. 8) that the stability of AFM/CO state may play a crucial role in the evolution of magnetic properties with a decrease of nanoparticles size. The C-type AFM structure observed in bulk $La_{0.2}Ca_{0.8}MnO_3$ manganite[23] is much more stable than the CE-type one characteristic for bulk $La_{0.4}Ca_{0.6}MnO_3$ (Ref. 2) and $Pr_{0.5}Ca_{0.5}MnO_3$ manganites.[8,36] For this reason, the OO state does not disappear even in smaller LCMO15 nanoparticles.

It was suggested for electron-doped manganite nanoparticles that the number of spins deviating from the AFM arrangement increases with reducing particle size, implying the increasing proportion of the uncompensated spins, which have a key role in exchange bias effect.[11] Thus, the uncompensated surface spins favor the FM coupling, leading to the formation of FM clusters and their growth with reducing particle size.[4,9,16] This explanation was based on Néel's suggestion[37] that the permanent moment of small AFM nanoparticles is attributed to incomplete magnetic compensation between spins in "up" and "down" sublattices. Néel also emphasized that the magnetic-moment dependence on particle size, which originated from uncompensated spins, is related to the crystal structure and to particle morphology. He considered three general cases for the number of uncompensated spins in small AFM nanoparticles, see also Refs. 38 and 39. If the uncompensated spins occur at random in the particle the number of uncompensated spins n should be proportional to $N^{1/2}$, where N is total number of spins in the particle. If particle consists of either an even or an odd number of planes with parallel spins, but with alternating magnetization directions, the number of uncompensated spins n should be rather proportional to $N^{2/3}$. In the third case as there is a random occupancy at the surface only, n is $\propto N^{1/3}$. Taking into account that N is proportional to D^3, where D is diameter of nanoparticle, magnetic moment M_{US} associated with the number of uncompensated spins should be equal to the ratio of n/N and proportional to $1/D^{1.5}$, $1/D$, and $1/D^2$, respectively. Sometimes, e.g., in Ref. 40, the authors assume that number of uncompensated spins is distributed over whole nanoparticle ($n \propto N^{1/2}$), whereas in other studies, e.g., in Ref. 41, it is suggested that more realistic seems a picture in which M_{US} has its main contribution from the surface ($n \propto N^{1/3}$). In order to find reliable description, we have fitted expression $M_0 = A/D^{\alpha}$ with two free parameters A and α to the experimental results of size variation of the FM moment. Results of the fitting with $A = 3.01 \pm 0.25$ and $\alpha = 0.43 \pm 0.02$ are given in the inset of Fig. 7. Unexpectedly,

results of the fitting show that M_0 decreases with increasing particle size even slower than that predicted by all of the above discussed models. Somewhat similar variation of M_0 with particle size was observed for $CoRh_2O_4$ nanoparticles,[42] though the authors did not discuss the exact form of M_0 vs D dependence. The particle-size dependence of spontaneous moment may for several reasons differ from that one predicted for known models.[37] The presence of two FM components which scales in different way with particle size may affect such a dependence. In this case it is impossible to distinguish between contribution from uncompensated spins inevitably existing in AFM nanoparticles and other contributions. This issue was discussed recently taking into account comparison of the uncompensated moments obtained for NiO nanoparticles by magnetometry with those obtained from the Mössbauer data.[41] Larger value obtained by magnetometry may be related to a particle-size distribution since signal in Mössbauer spectroscopy is weighted by the volume of the particles, whereas in magnetometry the signal is weighted by the moment.[41] Additional reason that affects M_0 and its variation with particle size may be magnetic interaction between nanoparticles.[41] At high particle densities, as shells come into contact and their effective thickness increases twice, apart from the classical dipole interaction, the exchange coupling between atoms belonging to neighboring particles, starts to play a role in the system.[39,43,44] Bahl *et al.*[41] estimated that for the clusters of strongly interacting particles, each containing p particles, the value of uncompensated moment obtained from magnetometry data will be larger than real value by factor of $\sqrt{p}$. For all above reasons it may appear that variation of spontaneous moment with particle size is not simple and cannot be attributed to the uncompensated spins only, see inset in Fig. 7. However, the issue is still open and more experimental work should be devoted to its clarification.

Slow relaxations following stretched exponential or logarithmic dependences were observed in various phase-separated perovskites. In many aspects, the dynamics of the phase-separated state of manganites resembles that of the spin glass.[1,29–32,45] It is worth noticing that a description of the phase-separated state as comprising two different phases is highly oversimplified.[45] While numerous studies clearly indicate that the phase-separated state in the phase-separated systems is not in thermodynamic equilibrium, the physical origin of the dynamical behavior is not fully understood. In order to explain relaxation dynamics in phase-separated perovskites, Rivadulla *et al.*[29] have proposed that the phase-separated state can be considered as a spin glass or a cluster-spin glass. In this case, an intercluster magnetic interaction brings upon collectivity among magnetic clusters. Alternative model to explain time-dependent effects in phase-separated manganites has been proposed by Levy *et al.*[46] In this model, the time dependence observed in magnetic and transport characteristics is attributed to the hindered kinetics of the low-temperature phase, where the boundaries of the phases relax through a hierarchy of energy barriers to attain equilibrium. Nevertheless, time-dependent behavior of magnetization observed for $La_{0.2}Ca_{0.8}MnO_3$ nanoparticles (Fig. 8) differs significantly from slow relaxation toward equilibrium. In highly concentrated samples with a random distribution of the easy axis and interparticle interactions, magnetic frustration may lead at low temperatures to a states of frozen particle's spins, apart from the effects of surface-to-core exchange coupling.[47] The main types of magnetic interactions that can be found in fine-particle assemblies are dipole-dipole interaction, which always exists, and the FM-like DE correlations appearing across the interface between two nanoparticles.[48] It seems that the origin of unusual time-dependent variation of magnetization with high level of the noise and the absence of clear tendency to saturation still remains enigmatic. Consequently, further detailed experiments are needed to verify character and nature of remarkable time-dependent dynamics of magnetization for nanoparticles of electron-doped manganites in magnetic field.

Let us discuss size-dependent EB effect observed in LCMO nanoparticles (Figs. 9–11). In a core-shell structure, the inner part of the particle, i.e., the core has the same properties as the bulk material, whereas the outer layer, namely, a shell, contains most of the oxygen faults and vacancies in the crystallographic structure. The appearance of M_0 at temperature significantly higher than T_N (Fig. 12) suggests that the magnetic structure of the nanoparticles is comprised of AFM core with size-dependent T_N and FM shell. If the FM shell is as thin as few lattice units, its spin magnetization may behave as in spin-glass-like layer.[11,15] Another unusual feature is the appearance of second FM component, presumable inside AFM core, that may also contribute to EB effect. Indeed, intrinsic interface-exchange coupling was revealed in bulk phase separated $Pr_{1/3}Ca_{2/3}MnO_3$ and $Y_{0.2}Ca_{0.8}MnO_3$ (Ref. 13) manganites and $RE_{1-x}Sr_xCoO_3$ [RE=La (Ref. 14) and Nd (Ref. 34)] cobaltites. For exchange-biased systems, it is generally assumed that T_C of the FM component has to be larger than T_N. It has been demonstrated recently in thin-film systems and AFM MnO nanoparticles with ferrimagnetic Mn_3O_4 shell that exchange bias can be induced in systems with $T_C < T_N$.[11,40,49] It appears that the magnetization in the paramagnetic state induced by the cooling in magnetic field and probably some local ordering of paramagnetic phase at the interface due to the AFM are sufficient to induce EB.[40,47,49,50] As pointed out already, linear correlation between M_{EB} and H_{EB} holds well for LCMO37 sample [Fig. 11(c)], while for smaller LCMO15 nanoparticles this relationship does not hold in the whole temperature range. The simple, albeit very qualitative, explanation may come out from different ratio of both contributions to exchange bias effect from two FM-like components. The comparison between spontaneous moments at 120 K [higher than T_C(on)] and M_0 at 10 K gives a ratio of 0.39 for LCMO15 and only 0.18 for LCMO37. Thus prevailing low-temperature FM-like contribution to EB in the case of LCMO37 displays usual linear correlation between M_{EB} and H_{EB}. For LCMO15, a relation between M_{EB} and H_{EB} is approximately linear for small values of these quantities and the competition between two comparable components of the EB may bend it away from the original slope at higher values of M_{EB} and H_{EB}. As for the temperature variation of H_{EB} and M_{EB} in LCMO37, both quantities vanish much below T_N and T_C(on) see Fig. 11(b). This is in contrast with results for LCMO15 [Fig. 11(b)], where small but well visible H_{EB} is observed above T_C(on), evidencing the contribution of high-temperature FM component to EB effect.

Alternative explanation of the disappearance of remanence and spontaneous magnetization at different temperatures may be advanced based only on one exchange coupling between AFM core and FM domains in the shell of nanoparticles. In this scenario low-temperature FM moment at T_C(on) could correspond to a slight canting of the spins of AFM phase. Then spin canting, coercivity, and exchange-bias progressively diminish with increasing temperature and fully disappear at approaching T_N, while surface ferromagnetism goes away only at $T \sim 200$ K.

IV. CONCLUSIONS

In summary, $La_{0.2}Ca_{0.8}MnO_3$ nanoparticles with average particle size from 15 to 37 nm, were prepared by recently proposed the glycine-nitrate method. The particles were characterized by XRD, TEM, and EDS data. The experimental data and the analysis of the results confirm the stability of the OO/AFM state. The results obtained were compared with the magnetic properties of the bulk $La_{0.2}Ca_{0.8}MnO_3$ counterpart. It is shown that the ferromagnetic moment attributed to the shell of the nanoparticles prevails at temperature as high as 200 K, while additional ferromagnetic component, that appear due to spin canting of antiferromagnetic phase or due to the presence of domains of orbitally disordered phase within antiferromagnetic core, emerges upon cooling. It is shown that ferromagnetic moment at low temperatures increases with decreasing particle size, but even in the smallest 15 nm particles the volume of the FM phase is only of about 0.8% at 5 K, signifying basically the antiferromagnetic ground state.

In contrast with bulk sample, the appearance of low-temperature FM component results in an appearance of cluster-glass-like features, such as a gap between ZFC and FC magnetization and significant frequency dependence of ac susceptibility. The time dependence of magnetization, recorded in magnetic fields ≥ 5 kOe after the field cooling, exhibits a very noisy behavior at low temperatures. This behavior may be attributed to the formation of collective state with no clear tendency to reach equilibrium state. Furthermore, upon field cooling, the particles display exchange bias effect. The temperature variation of bias field, remanent magnetization, and spontaneous magnetic moment with particle size is discussed in terms of the magnetic coupling between the antiferromagnetic core and the FM-like shell. These results are helpful to understand the evolution of the spin configuration in nanoparticles of electron-doped manganites.

ACKNOWLEDGMENTS

The authors thank V. Ezerskii for his help in TEM characterization. This work was supported in part by the Polish Ministry of Science and Higher Education under a research Project No. N N202 103736.

*Corresponding author; markoviv@bgu.ac.il

[1] E. Dagotto, *Nanoscale Phase Separation and Colossal Magnetoresistance*, Springer Series in Solid State Physics (Springer-Verlag, Berlin, 2003).

[2] J. B. Goodenough, in *Handbook on the Physics and Chemistry of Rare Earth*, edited by K. A. Gschneidner, Jr., J.-C. G. Bunzli, and V. Pecharsky (Elsevier Science, Amsterdam, 2003), Vol. 33.

[3] T. Sarkar, B. Ghosh, A. K. Raychaudhuri, and T. Chatterji, Phys. Rev. B **77**, 235112 (2008).

[4] T. Zhang, T. F. Zhou, T. Qian, and X. G. Li, Phys. Rev. B **76**, 174415 (2007).

[5] C. L. Lu, S. Dong, K. F. Wang, F. Gao, P. L. Li, L. Y. Lv, and J. M. Liu, Appl. Phys. Lett. **91**, 032502 (2007).

[6] S. S. Rao, S. Tripathi, D. Pandey, and S. V. Bhat, Phys. Rev. B **74**, 144416 (2006).

[7] A. Biswas and I. Das, Phys. Rev. B **74**, 172405 (2006).

[8] T. Zhang and M. Dressel, Phys. Rev. B **80**, 014435 (2009).

[9] S. Dong, F. Gao, Z. Q. Wang, J.-M. Liu, and Z. F. Ren, Appl. Phys. Lett. **90**, 082508 (2007); S. Dong, R. Yu, S. Yunoki, J. M. Liu, and E. Dagotto, Phys. Rev. B **78**, 064414 (2008).

[10] E. Rozenberg, M. Auslender, A. I. Shames, D. Mogilyansky, I. Felner, E. Sominskii, A. Gedanken, and Ya. M. Mukovskii, Phys. Rev. B **78**, 052405 (2008).

[11] J. Nogués, J. Sort, V. Langlais, V. Skumryev, S. Suriñach, J. S. Muñoz, and M. D. Baró, Phys. Rep. **422**, 65 (2005).

[12] D. Niebieskikwiat and M. B. Salamon, Phys. Rev. B **72**, 174422 (2005).

[13] T. Qian, G. Li, T. F. Zhou, X. Q. Xiang, X. W. Kang, and X. G. Li, Appl. Phys. Lett. **90**, 012503 (2007).

[14] Y. K. Tang, Y. Sun, and Z. H. Cheng, Phys. Rev. B **73**, 174419 (2006).

[15] V. Markovich, I. Fita, A. Wisniewski, R. Puzniak, D. Mogilyansky, L. Titelman, L. Vradman, M. Herskowitz, and G. Gorodetsky, Phys. Rev. B **77**, 054410 (2008).

[16] X. H. Huang, J. F. Ding, G. Q. Zhang, Y. Hou, Y. P. Yao, and X. G. Li, Phys. Rev. B **78**, 224408 (2008); X. H. Huang, J. F. Ding, Z. L. Jiang, Y. W. Yin, Q. X. Yu, and X. G. Li, J. Appl. Phys. **106**, 083904 (2009).

[17] M. Thakur, M. Patra, K. De, S. Majumdar, and S. Giri, J. Phys.: Condens. Matter **20**, 195215 (2008).

[18] M. Pissas and G. Kallias, Phys. Rev. B **68**, 134414 (2003); V. Likodimos and M. Pissas, J. Phys.: Condens. Matter **17**, 3903 (2005).

[19] C. D. Ling, E. Granado, J. J. Neumeier, J. W. Lynn, and D. N. Argyriou, Phys. Rev. B **68**, 134439 (2003); E. Granado, C. D. Ling, J. J. Neumeier, J. W. Lynn, and D. N. Argyriou, *ibid.* **68**, 134440 (2003).

[20] V. Markovich, I. Fita, R. Puzniak, E. Rozenberg, C. Martin, A. Wisniewski, Y. Yuzhelevski, and G. Gorodetsky, Phys. Rev. B **71**, 134427 (2005).

[21] D. Markovic, V. Kusigerski, M. Tadic, J. Blanusa, M. V. Antisari, and V. Spasojevic, Scr. Mater. **59**, 35 (2008).

[22] S. Kolesnik and B. Dabrowski, J. Supercond. **16**, 501 (2003).

[23] M. Pissas, G. Kallias, M. Hofmann, and D. M. Többens, Phys.

Rev. B **65**, 064413 (2002).
[24] A. I. Shames, E. Rozenberg, M. Auslender, G. Gorodetsky, C. Martin, A. Maignan, and Ya. M. Mukovskii, J. Magn. Magn. Mater. **290-291**, 910 (2005).
[25] A. H. Morrish, *Physical Principles of Magnetism* (Wiley, New York, 1965).
[26] J. A. Mydosh, *Spin Glasses* (Taylor & Francis, London, 1993).
[27] R. H. Kodama, A. E. Berkowitz, E. J. McNiff, and S. Foner, Phys. Rev. Lett. **77**, 394 (1996).
[28] *Surface Effects in Magnetic Nanoparticles*, edited by D. Fiorani (Kluwer, Dordrecht, 2005).
[29] F. Rivadulla, M. A. López-Quintela, and J. Rivas, Phys. Rev. Lett. **93**, 167206 (2004).
[30] J. Tao, D. Niebieskikwiat, M. B. Salamon, and J. M. Zuo, Phys. Rev. Lett. **94**, 147206 (2005).
[31] D. Niebieskikwiat, J. Tao, J. M. Zuo, and M. B. Salamon, Phys. Rev. B **78**, 014434 (2008).
[32] R. S. Freitas, L. Ghivelder, F. Damay, F. Dias, and L. F. Cohen, Phys. Rev. B **64**, 144404 (2001).
[33] N. Moutis, C. Christides, I. Panagiotopoulos, and D. Niarchos, Phys. Rev. B **64**, 094429 (2001).
[34] M. Patra, M. Thakur, S. Majumdar, and S. Giri, J. Phys.: Condens. Matter **21**, 236004 (2009).
[35] A. Sundaresan, R. Bhargavi, N. Rangarajan, U. Siddesh, and C. N. R. Rao, Phys. Rev. B **74**, 161306(R) (2006).
[36] Z. Jirák, F. Damay, M. Hervieu, C. Martin, B. Raveau, G. André, and F. Bourée, Phys. Rev. B **61**, 1181 (2000).
[37] L. Néel, Compt. Rend. Acad. Sci. Paris **252**, 4075 (1961); **253**, 9 (1961); **253**, 1286 (1961).
[38] J. T. Richardson, D. I. Yiagas, B. Turk, K. Forster, and M. V. Twigg, J. Appl. Phys. **70**, 6977 (1991).
[39] S. Mørup, D. E. Madsen, C. Frandsen, C. R. H. Bahl, and M. F. Hansen, J. Phys.: Condens. Matter **19**, 213202 (2007).
[40] G. Salazar-Alvarez, J. Sort, S. Surinãch, M. D. Baro, and J. Nogués, J. Am. Chem. Soc. **129**, 9102 (2007).
[41] C. R. H. Bahl, M. F. Hansen, T. Pedersen, S. Saadi, K. H. Nielsen, B. Lebech, and S. Mørup, J. Phys.: Condens. Matter **18**, 4161 (2006).
[42] R. N. Bhowmik, R. Nagarajan, and R. Ranganathan, Phys. Rev. B **69**, 054430 (2004).
[43] J. Nogués, V. Skumryev, J. Sort, S. Stoyanov, and D. Givord, Phys. Rev. Lett. **97**, 157203 (2006).
[44] M. F. Hansen, C. B. Koch, and S. Mørup, Phys. Rev. B **62**, 1124 (2000).
[45] M. Quintero, F. Parisi, G. Leyva, and L. Ghivelder, J. Phys.: Condens. Matter **20**, 345204 (2008).
[46] P. Levy, F. Parisi, L. Granja, E. Indelicato, and G. Polla, Phys. Rev. Lett. **89**, 137001 (2002).
[47] A. Labarta, X. Batlle, and O. Iglesias, in *Surface Effects in Magnetic Nanoparticles*, Springer Series Nanostructure Science and Technology, edited by D. Fiorani (Springer, New York, 2005).
[48] E. Rozenberg, A. I. Shames, M. Auslender, G. Jung, I. Felner, J. Sinha, S. S. Banerjee, D. Mogilyansky, E. Sominski, A. Gedanken, Ya. M. Mukovskii, and G. Gorodetsky, Phys. Rev. B **76**, 214429 (2007).
[49] A. E. Berkowitz, G. F. Rodriguez, J. I. Hong, K. An, T. Hyeon, N. Agarwal, D. J. Smith, and E. E. Fullerton, Phys. Rev. B **77**, 024403 (2008).
[50] X. W. Wu and C. L. Chien, Phys. Rev. Lett. **81**, 2795 (1998).